Hadronic resonance production with ALICE at the LHC

Sergey Kiselev[*] **for the ALICE collaboration**

Institute for Theoretical and Experimental Physics, Moscow, Russia
E-mail: Sergey.Kiselev@cern.ch

The hadronic resonances $K^*(892)^0$ and $\phi(1020)$ have been measured by the ALICE experiment at the LHC in pp, p–Pb and Pb–Pb collisions. Transverse momentum spectra, yields, ratio to stable particles, nuclear modification factors and comparison with model predictions are discussed. The ALICE results are compared with data obtained at lower energies.

---

[*]Speaker.

1. Introduction

Resonance production plays an important role both in elementary and in heavy-ion collisions. In pp and p–A collisions, it provides the baseline for heavy-ion collisions and it can be used to study system size dependence and the role of cold nuclear matter. In heavy-ion collisions, it contributes to the systematic study of in-medium parton energy loss and its flavor dependence. Moreover, effects related to the high density and/or high temperature of the medium can modify the properties of short-lived resonances such as their masses, widths, and even their spectral shapes [1]. In the final hadronic stage of the collision, due to short lifetime, regeneration and rescattering effects become important and can be used to estimate the timescale between chemical and kinetic freeze-out [2]. Results for $K^*(892)^0$ ($c\tau \sim 4$ fm) and $\phi(1020)$ ($c\tau \sim 45$ fm) short-lived resonances measured by ALICE in pp, p–Pb and Pb–Pb collisions are presented at this seminar.

2. The ALICE detector

The ALICE detector [3] [4] at the LHC is designed to study both Pb–Pb and pp collisions at the TeV-scale center of mass energy. The components of the ALICE detector most directly related to the results presented here are shortly described below. The Inner Tracking System (ITS) is a silicon detector that surrounds the interaction point and covers the pseudorapidity region $|\eta| < 0.9$. It is used to reconstruct the collision vertex and provides tracking and particle identification. Particle tracking is mainly provided by Time Projection Chamber (TPC). The TPC also allows particles to be identified through their energy loss. The Time-of-Flight Detector (TOF) sits after the TPC and measures the time-of-flight of the particles, allowing for additional identification. Both the TPC and the TOF cover the central pseudorapidity region $|\eta| < 0.9$. A pair of scintillation hodoscopes, covering $2.8 < \eta < 5.1$ (VZERO-A) and $-3.7 < \eta < -1.7$ (VZERO-B), were used for event triggering and event selection (centrality, multiplicity) in Pb–Pb and p–Pb collisions.

3. Analysis Procedure

The resonances have been reconstructed via their main hadronic decay channel: $K^*(892)^0 \rightarrow \pi^\pm + K^\mp$, $\phi(1020) \rightarrow K^+ + K^-$. Due to their very short lifetime, resonance decay products cannot be distinguished from the particles coming from the primary vertex, and their yield can only be measured by first computing the invariant mass spectrum of all primary candidate's track pairs and then subtracting the combinatorial background. The combinatorial background was evaluated using the event-mixing technique or the like-sign technique. The signal after the combinatorial background subtraction was then fitted with a Breit-Wigner function for K^{*0} or a Voigtian function (convolution of Breit-Wigner and Gaussian which accounts for the detector resolution) for ϕ plus a polynomial for the residual background[1]. After the signal is extracted, the raw yield is evaluated as the integral of the signal function. The raw yields extracted in different p_T bins are corrected for efficiency and acceptance and the differential transverse momentum spectra are obtained. The corrected spectra are fitted with a Levy-Tsallis function [5] (pp and p–Pb collisions) or with a Blast Wave function [6] (Pb–Pb collisions), in order to extract the mean transverse momentum $\langle p_T \rangle$ and

---

[1]We denote by K^{*0} the average of $K^*(892)^0$ and $\overline{K}^*(892)^0$ and by ϕ the $\phi(1020)$ meson

p_T-integrated yields. These quantities have been measured for pp collisions at $\sqrt{s}$ = 0.9 [7], 2.76 and 7 TeV [8], p–Pb collisions at $\sqrt{s_{NN}}$ = 5.02 TeV and Pb–Pb collisions at $\sqrt{s_{NN}}$ = 2.76 TeV [9].

4. Results

Examples of the invariant mass spectra for Pb–Pb [9] and p–Pb collisions are presented in Fig. 1. Masses and widths of resonances are close to the PDG values [10], as illustrated in Fig. 2 for
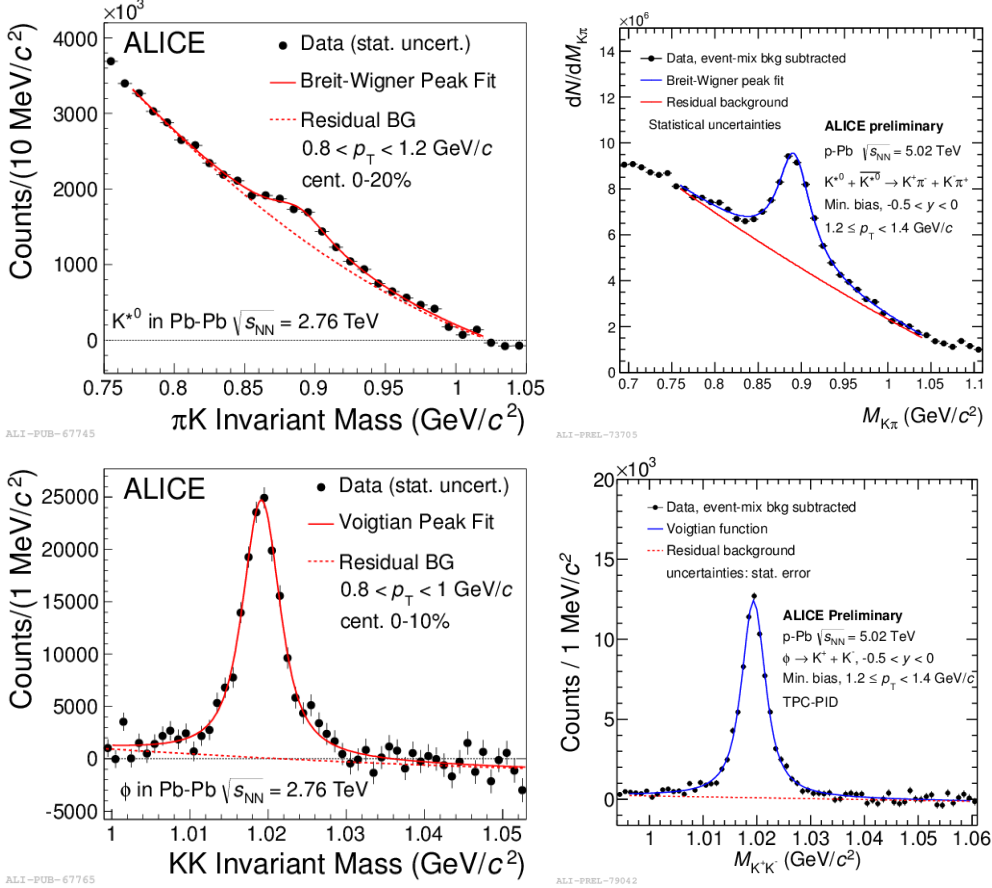
Figure 1: (color online) Signals after the combinatorial background subtraction for Pb–Pb (left) [9] and p–Pb (right) collisions. The fitting function is the sum of a Breit-Wigner function for K^{*0} (top) or a Voigtian function for ϕ (bottom) and a polynomial.

Pb–Pb collisions [9]. Pb–Pb data obtained in 2011 let us to extend measured p_T region of spectra published in [9] up to 10 and 21 GeV/c for K^{*0} and ϕ respectively, as shown in Fig. 3. Figure 4 shows K^{*0} and ϕ spectra in p–Pb collisions at $\sqrt{s_{NN}}$ = 5.02 TeV in different event multiplicity classes.

Figure 5 shows $\langle p_T \rangle$ for the K^{*0} and ϕ resonances as a function of the mean number of participating nucleons $\langle N_{part} \rangle$. For central collisions $\langle p_T \rangle$ of the $K^{*0}(\phi)$ resonance measured in Pb–Pb collisions at $\sqrt{s_{NN}}$ = 2.76 TeV is about 20% (30%) higher than the values measured in Au–Au
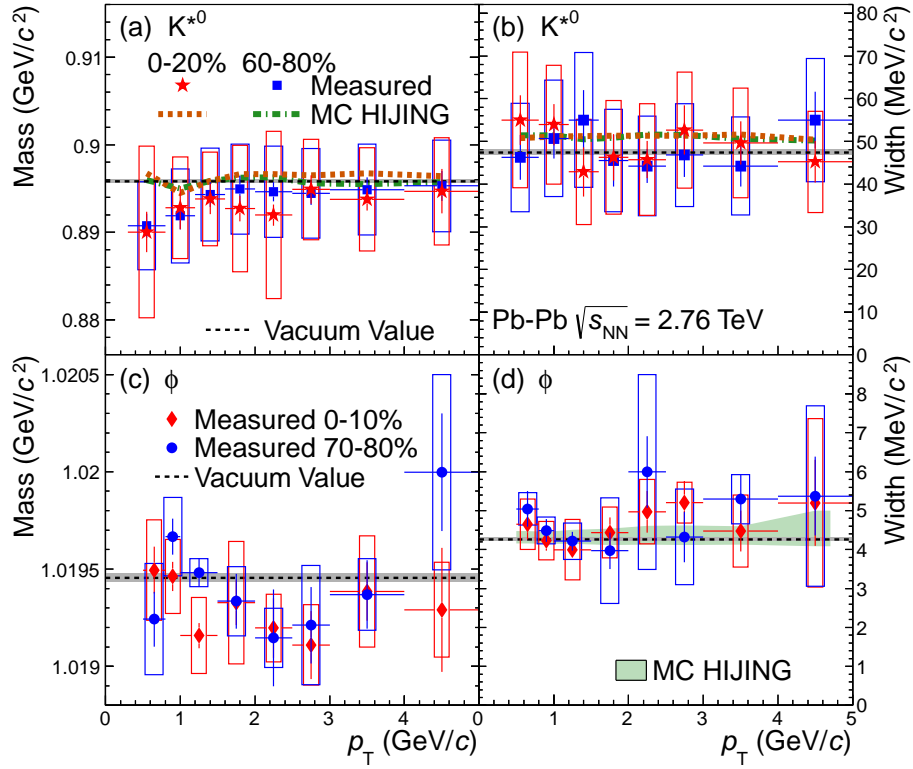
Figure 2: (color online) Mass (left) and width (right) of the K^{*0} (top) and ϕ (bottom) in Pb–Pb collisions at $\sqrt{s_{NN}} = 2.76$ TeV as a function of transverse momentum [9].
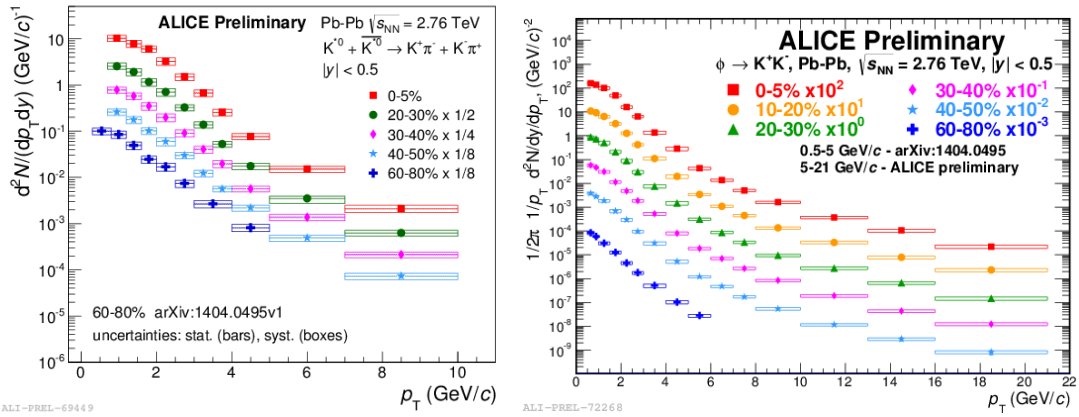
Figure 3: (color online) K^{*0} (left) and ϕ (right) invariant transverse momentum spectra in Pb–Pb collisions at $\sqrt{s_{NN}} = 2.76$ TeV in different centrality intervals.
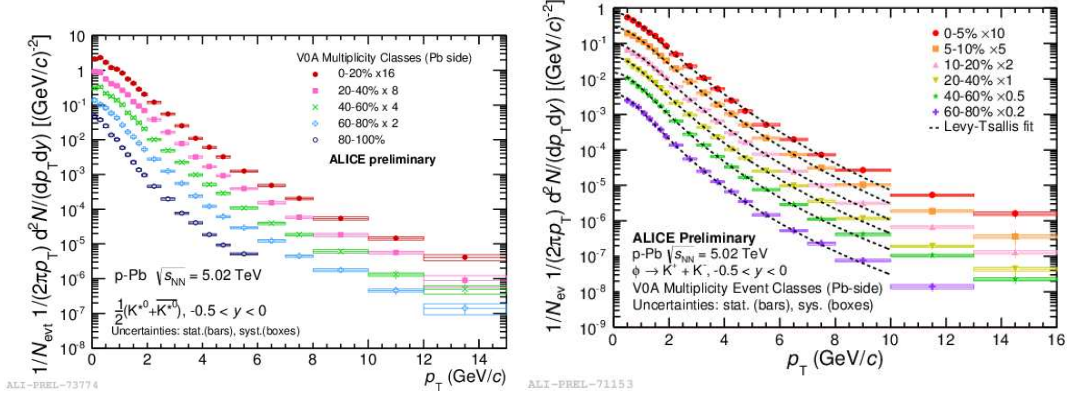
Figure 4: (color online) K^{*0} (left) and ϕ (right) invariant transverse momentum spectra in p–Pb collisions at $\sqrt{s_{NN}} = 5.02$ TeV in different event multiplicity classes.

collisions at $\sqrt{s_{NN}} = 200$ GeV. This is consistent with the observation [11] of increased radial flow in A–A collisions at the LHC relative to RHIC.
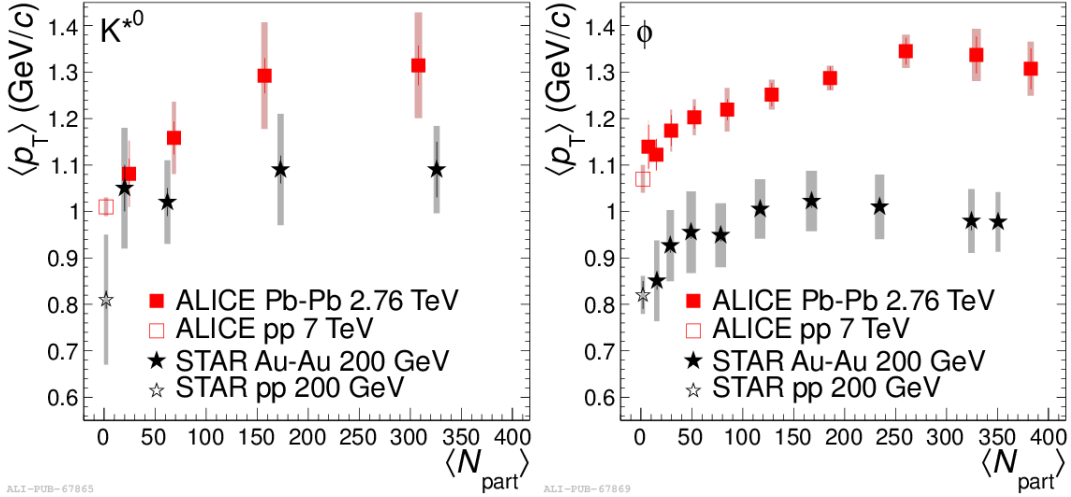
Figure 5: (color online) Mean transverse momentum of the K^{*0} (left) and ϕ (right) resonances as a function of the mean number of participating nucleons $\langle N_{part} \rangle$ in Pb–Pb collisions at $\sqrt{s_{NN}} = 2.76$ TeV [9]. The results are compared with the pp measurements at $\sqrt{s} = 7$ TeV and also with the lower energy measurements at RHIC.

In Pb–Pb collisions the $\langle p_T \rangle$ values of the K^{*0} and ϕ resonances demonstrate similar increasing trend with multiplicity as other hadrons, as shown in Fig. 6. Moreover, mass ordering is observed in central Pb–Pb collisions. The K^{*0}, p and ϕ, which have similar masses, are observed to have similar $\langle p_T \rangle$ values. This is consistent with hydrodynamic picture. Also in p–Pb collisions the $\langle p_T \rangle$ of resonances increases as a function of the average charged particle multiplicity density, as for other hadrons, Fig. 7. However, while $\langle p_T \rangle$ of stable hadrons approximately follows mass ordering, the $\langle p_T \rangle$ of K^{*0} and ϕ is found to be larger than of protons. A similar trend is observed

5
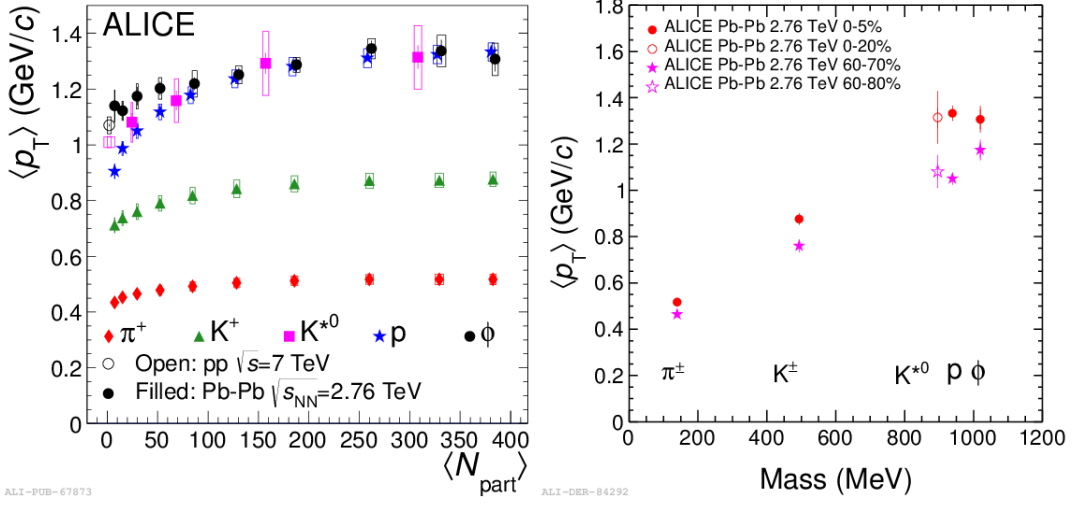
Figure 6: (color online) Mean transverse momentum of the K^{*0}, ϕ mesons and stable hadrons as a function of the mean number of participating nucleons $\langle N_{\text{part}} \rangle$ (left) [9] and the particle mass (right) in Pb–Pb collisions at $\sqrt{s_{\text{NN}}} = 2.76$ TeV.

in pp collisions at 7 TeV: $\langle p_T \rangle_\phi > \langle p_T \rangle_{K^{*0}} > \langle p_T \rangle_p$. The question is open whether the mesonic resonances deviate from mass ordering or the baryons do instead.
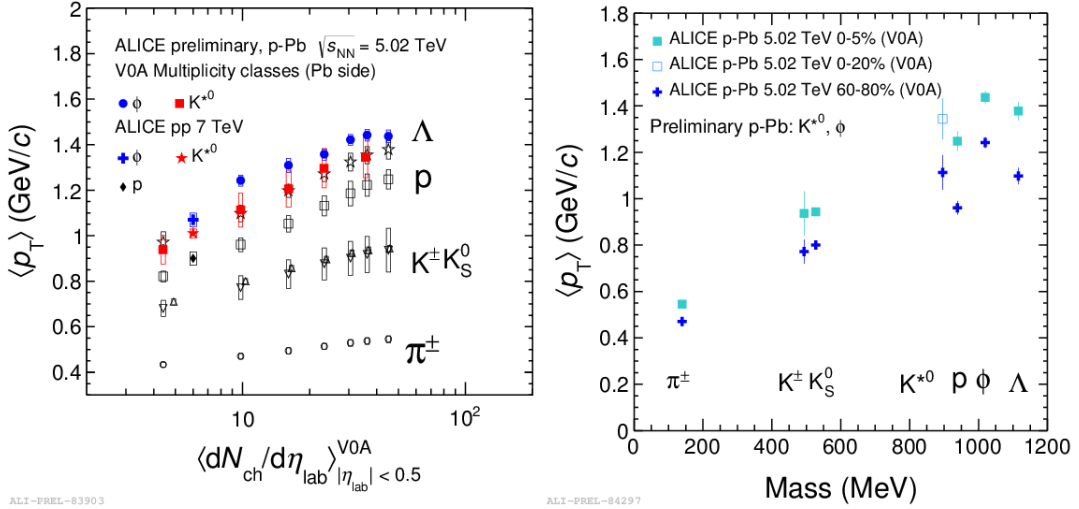
Figure 7: (color online) Mean transverse momentum of the K^{*0}, ϕ mesons and stable hadrons as a function of the average charged particle multiplicity density (left) and the particle mass (right) in p–Pb collisions at $\sqrt{s_{\text{NN}}} = 5.02$ TeV.

Figure 8 shows the $\langle p_T \rangle$ of K^{*0}, p and ϕ as a function of the system size in the three collision systems. The $\langle p_T \rangle$ of resonances in p–Pb shows a steeper increase with multiplicity than in Pb–Pb, as also observed for stable hadrons [12].

Figure 9 (left) presents the particle ratios K^{*0}/K^- and ϕ/K^- as a function of the system size
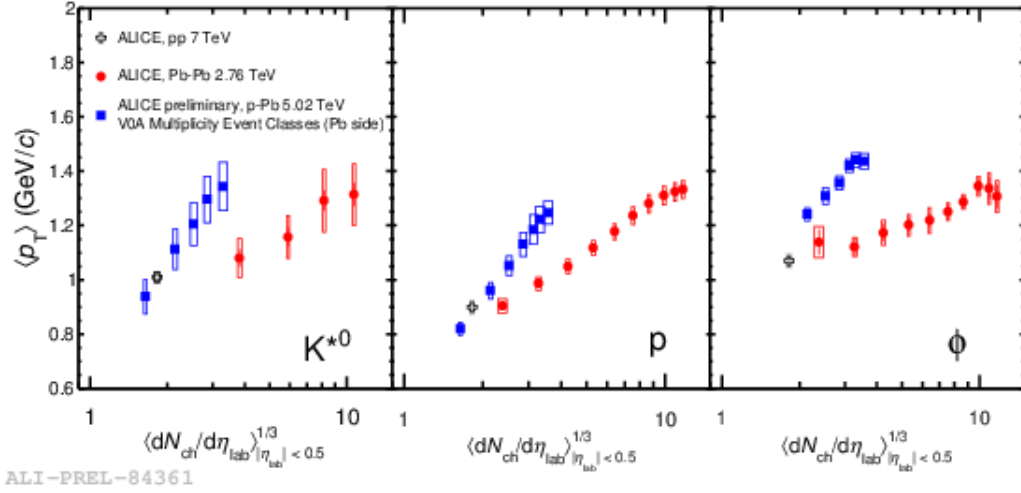
Figure 8: (color online) System size dependence of the mean transverse momentum of the K^{*0}, p and ϕ. The system size is defined as the cubic root of the average charged particle multiplicity density.

in pp, p–Pb and Pb–Pb collisions. The K^{*0}/K^- ratio exhibits a decreasing trend towards more
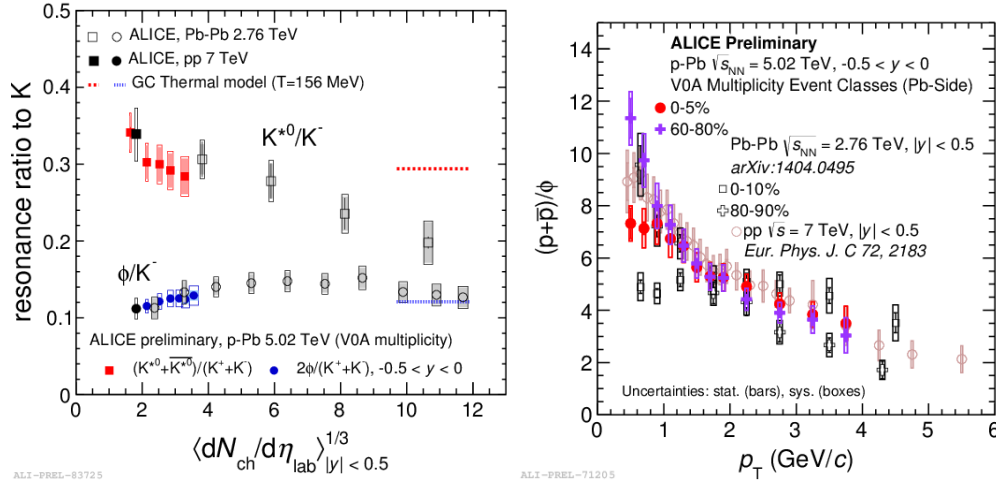
Figure 9: (color online) (left) Ratio of resonances to charged kaons as a function of the system size in the three collision systems [9]. (right) $(p+\overline{p})/\phi$ ratio as a function of transverse momentum in the three collision systems.

central Pb–Pb collisions, where the measured ratio is about 60% of the thermal model prediction with T = 156 MeV [13]. This suppression is consistent with rescattering of K^{*0} daughters in the hadronic phase of central collisions as the dominant effect. As described in [9], the K^{*0}/K^- ratio measured in central Pb–Pb collisions can be used along with the thermal model with rescattering effect [2] to obtain an estimate of 2 fm/c for the lower limit of the time between chemical and kinetic freeze-out. In p–Pb collisions, the K^{*0}/K^- ratio sits along the extrapolation from pp to

peripheral Pb–Pb collisions. The ϕ/K^- ratio is nearly flat and agrees with the prediction of the thermal model. This suggests that rescattering effects are not important for ϕ, which has 10 times longer lifetime than K^{*0}.

Figure 9 (right) shows the $(\mathrm{p}+\bar{\mathrm{p}})/\phi$ ratio as a function of transverse momentum in pp, p–Pb and Pb–Pb collisions. For central Pb–Pb collisions the ratio is flat for $p_{\mathrm{T}} < 3\text{-}4$ GeV/c. This is consistent with hydrodynamic description: the shape of a spectrum is determined by the particle mass. The ratio in peripheral Pb–Pb collisions decreases steeply with p_{T}. For peripheral p–Pb and pp collisions the ratio is quantitatively consistent, with a trend similar to peripheral Pb–Pb collisions. For central p–Pb collisions the ratio shows a possible flattening for $p_{\mathrm{T}} < 1.5$ GeV/c, which could be interpreted as a hint for the onset of collective behavior in these collisions.

Figure 10 (left) shows the nuclear modification factors of the K^{*0} and ϕ resonances and stable hadrons as a function of p_{T} for central Pb–Pb collisions at $\sqrt{s_{\mathrm{NN}}} = 2.76$ TeV. At high p_{T} both
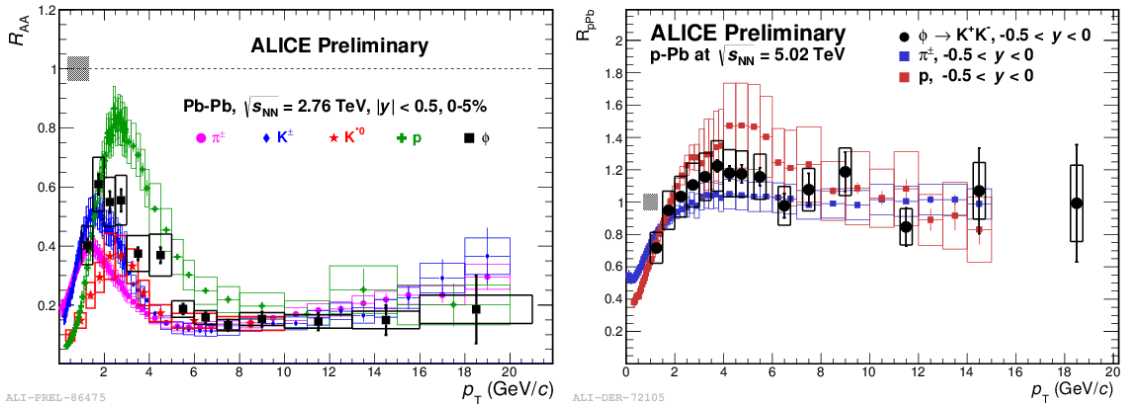
Figure 10: (color online) Nuclear modification factor of resonances and stable hadrons as a function of transverse momentum for central Pb–Pb collisions at $\sqrt{s_{\mathrm{NN}}} = 2.76$ TeV (left) and for minimum bias p–Pb collisions at $\sqrt{s_{\mathrm{NN}}} = 5.02$ TeV (right).

K^{*0} and ϕ strongly suppressed with respect to pp collisions, $R_{AA} \approx 0.15$ - 0.2. The suppression is consistent with that measured for the stable hadrons, supporting the flavor-independence of partonic energy loss in the medium. At intermediate p_{T}, $2 < p_{\mathrm{T}} < 6$ GeV/c, $R_{AA}(\pi^{\pm}, \mathrm{K}^{\pm}, \mathrm{K}^{*0}) < R_{AA}(\phi) < R_{AA}(\mathrm{p})$. At low p_{T}, $p_{\mathrm{T}} < 2$ GeV/c, the K^{*0} is more suppressed than charged hadrons, which may be an indication that rescattering effects are important. Figure 10 (right) shows the nuclear modification factors of the ϕ meson and stable hadrons in minimum bias p–Pb collisions at $\sqrt{s_{\mathrm{NN}}} = 5.02$ TeV. There is no suppression at high p_{T}, R_{pPb} does not deviate from unity for $\pi^{\pm}$, p and ϕ. At intermediate p_{T} there is a moderate Cronin peak.

5. Conclusions

The K^{*0} and ϕ resonance production have been measured in a wide momentum range in pp, p–Pb and Pb–Pb collisions by the ALICE experiment at the LHC. The masses and widths of the resonances are close to the PDG values. In pp and p–Pb collisions the resonance $\langle p_{\mathrm{T}} \rangle$ does not follow the same mass ordering as in central Pb–Pb collisions. The $\mathrm{K}^{*0}/\mathrm{K}^-$ ratio exhibits a significant

suppression going from peripheral to most central Pb–Pb collisions, consistent with rescattering of K^{*0} decay daughters in the hadronic phase due to short lifetime of K^{*0}. The ϕ/K^- ratio is not suppressed due to its longer lifetime. In central Pb–Pb collisions the $(p+\overline{p})/\phi$ ratio is flat for $p_T < 3$-4 GeV/c, which is consistent with hydrodynamic description. For central p–Pb collisions the ratio demonstrates a possible flattening for $p_T < 1.5$ GeV/c, which could be interpreted as a hint for the onset of collective behavior in these collisions. In central Pb–Pb collisions the nuclear modification factor R_{AA} of K^{*0} and ϕ resonances are strongly suppressed at high-p_T, consistent with the suppression for stable hadrons. There is no suppression at high p_T in minimum bias p–Pb collisions, R_{pPb} does not deviate from unity for $\pi^{\pm}$, p and ϕ.

References

[1] G. E. Brown and M. Rho, Phys. Rev. Lett. **66**, (1991) 2720. R. Rapp, Nucl. Phys. A **725**, (2003) 254. E. V. Shuryak and G. Brown, Nucl. Phys. A **717**, (2003) 322.

[2] G. Torrieri and J. Rafelski, Phys. Lett. B **509**, (2001) 239. J. Rafelski, J. Letessier and G. Torrieri, Phys. Rev. C **64** (1993) 054907. C. Markert, J. Rafelski and G. Torrieri, arXiv:0206260 [hep-ph].

[3] K. Aamodt *et al.*, (ALICE Collaboration), JINST **3**, (2008) S08002.

[4] B. Abelev *et al.*, (ALICE Collaboration), Int. J. Mod. Phys. A **29** (2014) 1430044.

[5] C. Tsallis, J. Stat. Phys. **52**, (1988) 479.

[6] E. Schnedermann, J. Sollfrank and U. Heinz, Phys. Rev. C **48** (1993) 2462

[7] K. Aamodt *et al.*, (ALICE Collaboration), Eur. Phys. J. C **71** (2011) 1594.

[8] K. Aamodt *et al.*, (ALICE Collaboration), Eur. Phys. J. C **72** (2012) 2183.

[9] B. Abelev *et al.*, (ALICE Collaboration), arXiv:1404.0495 [hep-ex].

[10] J. Beringer *et al.*, (Particle Data Group), Phys. Rev. D **86**, (2012) 010001.

[11] B. Abelev *et al.*, (ALICE Collaboration), Phys. Rev. C **88**, (2013) 044910.

[12] B. Abelev *et al.*, (ALICE Collaboration), Phys. Lett. B **727**, (2013) 371.

[13] J. Stachel *et al.*, J. Phys.: Conf. Ser. **509**, (2014) 012019.